# Testing general relativity with the reflection spectrum of the supermassive black hole in 1H0707−495

Zheng Cao,[1] Sourabh Nampalliwar,[1,2] Cosimo Bambi,[1,2,*] Thomas Dauser,[3] and Javier A. García[4,3,5]

[1] *Center for Field Theory and Particle Physics and Department of Physics, Fudan University, 200433 Shanghai, China*
[2] *Theoretical Astrophysics, Eberhard-Karls Universität Tübingen, 72076 Tübingen, Germany*
[3] *Remeis Observatory & ECAP, Universität Erlangen-Nürnberg, 96049 Bamberg, Germany*
[4] *Cahill Center for Astronomy and Astrophysics, California Institute of Technology, Pasadena, CA 91125, United States*
[5] *Harvard-Smithsonian Center for Astrophysics, Cambridge, MA 02138, United States*

(Dated: September 4, 2017)

Recently, we have extended the X-ray reflection model RELXILL to test the spacetime metric in the strong gravitational field of astrophysical black holes. In the present work, we employ this extended model to analyze *XMM-Newton*, *NuSTAR*, and *Swift* data of the supermassive black hole in 1H0707−495 and test deviations from a Kerr metric parametrized by the Johannsen deformation parameter $\alpha_{13}$. Our results are consistent with the hypothesis that the spacetime metric around the black hole in 1H0707−495 is described by the Kerr solution.



In 4-dimensional general relativity, the no-hair theorem guarantees that the only stationary and asymptotically flat vacuum black hole solution, which is regular on and outside the event horizon, is the Kerr metric [1]. It is also remarkable that the spacetime around astrophysical black holes formed by complete gravitational collapse in the Universe should be well approximated by the Kerr geometry [2]. Nevertheless, general relativity has been mainly tested in weak gravitational fields, in particular with Solar System experiments and radio observations of binary pulsars [3]. The strong gravity regime is largely unexplored, and there are a number of scenarios beyond Einstein's gravity that provide the same predictions for weak fields and present differences when gravity becomes strong.

The study of the properties of the electromagnetic radiation emitted by the gas in the accretion disk can potentially probe the spacetime metric around astrophysical black holes and test the Kerr nature of these objects [4]. Previous work has shown that X-ray reflection spectroscopy (the so-called iron line method) [5] is a promising technique to do this job [6]. Currently, the most advanced X-ray reflection model to describe the spectrum from the strong gravity region of a Kerr black hole is RELXILL [7]. In Ref. [8], we have described RELXILL_NK, an extension of RELXILL to non-Kerr spacetimes, and we have shown with some simulations how this new model can test the nature of astrophysical black holes. In this Letter, we employ RELXILL_NK for the first time to analyze real data and constrain possible deviations from the Kerr solution.

Let us first briefly review the physics and astrophysics behind X-ray reflection spectroscopy. Within the disk-corona model [9], an accreting black hole is surrounded by a geometrically thin and optically thick disk. The corona is a hotter cloud near the black hole. For instance, it might be the base of the jet, the atmosphere above the inner part of the disk, or some accreting material between the disk and the black hole. Its geometry is currently unknown. Because of inverse Compton scattering of thermal photons from the disk off free electrons in the corona, the latter becomes an X-ray source with a power-law spectrum. The corona also illuminates the disk, producing a reflection component with some fluorescent emission features, the most prominent of which is usually the iron K$\alpha$ line, which is at 6.4 keV in the case of neutral and weakly ionized iron and shifts up to 6.97 keV for H-like iron ions. Due to gravitational redshift, Doppler boosting, and light bending, the reflection spectrum is detected in the flat faraway region with a shape different from that at the emission point, and encodes all the details about the strong gravity region near the black hole [4].

There are two natural approaches to test the Kerr black hole hypothesis [2]. In the so-called top-down approach, we consider a specific alternative theory of gravity in which black holes are not described by the Kerr metric and we check whether astrophysical data prefer the Kerr or that non-Kerr metric. There are two problems to follow this method. First, there are a large number of alternative theories of gravity, and none seems to be more motivated than others, so we should repeat the analysis for every theory. Second, rotating black hole solutions in alternative theories of gravity are known only in quite exceptional cases, while the non-rotating or slow-rotating solutions are not very useful to test astrophysical black holes because the spin plays an important role in the shape of the spectrum.

In the bottom-up approach, we employ a phenomenological test-metric in which possible deviations from the Kerr solution are quantified by one or more "deformation parameters". The Kerr metric is recovered when all the deformation parameters vanish, and we want to check whether astrophysical data require vanishing deformation parameters; that is, if astrophysical black holes are indeed the Kerr black holes as expected in Einstein's gravity. In this Letter, as an explorative study, we follow

* Corresponding author: bambi@fudan.edu.cn

this bottom-up approach and we employ the Johannsen metric with the deformation parameter $\alpha_{13}$ [10]. The line element in Boyer-Lindquist coordinates reads (we use units in which $G_{\rm N} = c = 1$)

$$\begin{aligned} ds^2 = &-\frac{\Sigma\left(\Sigma - 2Mr\right)}{A^2}\,dt^2 + \frac{\Sigma}{\Delta}\,dr^2 + \Sigma\,d\theta^2 \\ &+ \frac{\left[\left(r^2+a^2\right)^2\left(1+\delta\right)^2 - a^2\Delta\sin^2\theta\right]\Sigma\sin^2\theta}{A^2}\,d\phi^2 \\ &- \frac{2a\left[2Mr + \delta\left(r^2+a^2\right)\right]\Sigma\sin^2\theta}{A^2}\,dt\,d\phi\,, \end{aligned} \tag{1}$$

where $a = J/M$, $\Sigma = r^2 + a^2\cos^2\theta$, $\Delta = r^2 - 2Mr + a^2$, and

$$A = \Sigma + \delta\left(r^2+a^2\right)\,, \quad \delta = \alpha_{13}\left(\frac{M}{r}\right)^3\,. \tag{2}$$

The Kerr metric is recovered when $\alpha_{13} = 0$. In order to have a regular exterior region (no singularities or closed time-like curves), we have to impose the following restriction to the value of $\alpha_{13}$ [10]

$$\alpha_{13} \geq -\left(1 + \sqrt{1-a_*^2}\right)^3\,, \tag{3}$$

where $a_* = a/M$ is the dimensionless spin parameter.

The supermassive black hole in the Narrow Line Seyfert 1 galaxy 1H0707−495 looks quite a promising source for testing the Kerr metric using X-ray reflection spectroscopy. Its spectrum has significant edge features, which are commonly interpreted as an extremely strong reflection component. Previous studies that assumed the Kerr metric found the inner edge of the accretion disk very close to the black hole (thus increasing the relativistic effects in the spectrum), a moderate inclination angle, and an extremely high iron abundance [11–14].

*XMM-Newton*, *NuSTAR*, and *Swift* observations of 1H0707−495 are shown in Tab. I. In our study, for *XMM-Newton* we have only considered the observation in 2011: it corresponds to the lowest flux state ever observed possessing clear edge features. For the same reason, the 2011 observation has been investigated by several authors, which is helpful for the choice of the models and the comparison of the results. The three separated observations of *NuSTAR* in 2014 have simultaneous snapshots of *Swift*. However, the second *Swift* observation was taken during an anomaly period of this mission and therefore was not included in our analysis. A brief description of the data reduction is reported in the Supplemental Material.

We have performed three separated studies (named Analysis 1, 2, and 3) employing the following models respectively

$$\begin{aligned} &\text{Model 1: TBABS*(RELXILL\_NK+DISKBB)}\,, \\ &\text{Model 2: TBABS*(RELXILL\_NK+RELXILL\_NK)}\,, \\ &\text{Model 3: TBABS*RELXILL\_NK}\,. \end{aligned} \tag{4}$$

Our results are summarized in Tab. II and in Figs. 1 and 2. The reflection spectrum of the disk in the Johannsen metric is described by RELXILL_NK, in which the free parameters are the black hole spin $a_*$, the deformation parameter $\alpha_{13}$, the inclination angle of the disk $i$, the emissivity index $q$ assuming a simple power-law $1/r^q$ where $r$ is the radial coordinate, the photon index of the primary component from the corona $\Gamma$, the ionization of the disk $\log\xi$, and the iron abundance $A_{\rm Fe}$ (in Solar units). TBABS takes the galactic dust absorption into account and the column number density has been set to the value measured for 1H0707−495 ($N_{\rm H} = 5.8\cdot10^{20}$ cm$^{-2}$) [14].

| Mission | Obs. ID | Year | Exposure (ks) |
|---|---|---|---|
| *XMM-Newton* | 0511580101 | 2008 | 124 |
| | 0511580201 | 2008 | 124 |
| | 0511580301 | 2008 | 123 |
| | 0511580401 | 2008 | 122 |
| | 0653510301 | 2010 | 117 |
| | 0653510401 | 2010 | 128 |
| | 0653510501 | 2010 | 128 |
| | 0653510601 | 2010 | 129 |
| | 0554710801 | 2011 | 98 |
| *NuSTAR* | 60001102002 | 2014 | 144 |
| | 60001102004 | 2014 | 49 |
| | 60001102006 | 2014 | 47 |
| *Swift* | 00080720001 | 2014 | 20 |
| | 00080720003 | 2014 | 17 |
| | 00080720004 | 2014 | 17 |

TABLE I. Observations of 1H0707−495. In this work, we have only considered the *XMM-Newton* observation of 2011, the three *NuSTAR* observations, and the first and the third *Swift* observations.

In Analysis 1, we have fitted the *XMM-Newton* EPIC-pn data with Model 1. We have employed DISKBB to fit the "soft excess" around 1 keV as done in Ref. [12]. The corresponding constraint on the spin and the deformation parameters are shown in the left panel in Fig. 1, where the red, green, and blue lines indicate, respectively, the 68%, 90%, and 99% confidence level curves.

In Analysis 2, we have fitted the same *XMM-Newton* data with Model 2 following what was done with a Kerr metric in Refs. [12, 14]. The double reflection model is one of the most popular models to fit the soft excess in AGN like 1H0707−495 in which the soft spectrum changes significantly with the flux state. There are a few possible physical explanations; for example, it could describe an inhomogeneous accretion disk. The parameters of the two reflection models are tied with the exception of the ionization, the iron abundance, and the normalization. The corresponding constraint on $a_*$ and $\alpha_{13}$ are shown in the right panel in Fig. 1.

The minimum of the reduced $\chi^2$ is not very close to 1 for Analysis 1 and Analysis 2. This is because the *XMM-Newton* data have very high signal to noise ratio below 1.5 keV and any model that cannot perfectly fit the soft excess has a relatively large reduced $\chi^2$ (see Ref. [15]

| | Analysis 1 | Analysis 2 | Analysis 3 | |
|---|---|---|---|---|
| Data | *XMM-Newton* 2011 | *XMM-Newton* 2011 | *NuSTAR*+*Swift* | |
| Model | 1 | 2 | 3 | |
| $a_*$ | $0.96^{+0.01}_{-0.08}$ | $> 0.98$ | $> 0.99$ | RELXILL_NK |
| $\alpha_{13}$ | $-0.8$ | $-0.05$ | $-0.66$ | |
| $i$ [deg] | $38^{+4}_{-7}$ | $49^{+2}_{-2}$ | $41^{+2}_{-3}$ | |
| $q$ | $3.6^{+1.1}_{-0.4}$ | $3.9^{+0.5}_{-0.5}$ | $3.7^{+0.1}_{-0.1}$ | |
| $\Gamma$ | $1.33^{+0.07}_{-0.10}$ | $2.49^{+0.03}_{-0.02}$ | $3.29^{+0.02}_{-0.01}$ | |
| | | | $2.59^{+0.04}_{-0.02}$ | |
| | | | $3.13^{+0.06}_{-0.01}$ | |
| $\log \xi$ | $< 1.79$ | $1.29^{+0.02}_{-0.05}$ | $2.15^{+0.24}_{-0.07}$ | |
| $A_{\rm Fe}$ | $> 8.6$ | $> 9.3$ | $> 9.6$ | |
| $T_{\rm in}$ | $0.150 \pm 0.003$ | | | DISKBB |
| $\log \xi'$ | | $3.30^{+0.01}_{-0.06}$ | | RELXILL_NK |
| $A'_{\rm Fe}$ | | $> 9.6$ | | |
| $\chi^2$/dof | $127/94 = 1.35$ | $157/94 = 1.67$ | 1938/3246 (C-stat/dof) | |

TABLE II. Summary of the best-fit values. The row Data indicates which observations have been used, and the numbers refer to those in Tab. I. The row Model indicates the Xspec model employed, and the number refers to that in Eq. (4). The reported uncertainty corresponds to the 90% confidence level for one relevant parameter. In Analysis 3, we have used the Cash-statistics instead of the $\chi^2$ one. See the text for more details.

for a discussion on this point). The residuals between 1 and 4 keV might be due, for example, to a highly ionized outflowing wind [13]. We could obtain a reduced $\chi^2$ closer to 1 excluding data below 1 or 1.5 keV, as done in some of previous studies in the literature [15]. Note, however, that the difficulty to fit the soft energy band is not crucial in the present study, whose goal is to test the Kerr metric and constrain on the deformation parameter $\alpha_{13}$, because our results are mainly sensitive to the iron K$\alpha$ complex, which is at higher energies. Note the fit is driven by the small error bars form the soft energy band.

Lastly, in Analysis 3 we have fitted the *NuSTAR* and *Swift* data with Model 3 following the study in the Kerr metric in Ref. [14]. We impose that the values of the model parameters are the same for the three observations, with the exception of the photon index $\Gamma$, as done in [14]. Note that in Analysis 3 we have used the Cash-statistics because of low photon count. The constraint on $\alpha_{13}$ is shown in Fig. 2.

In Ref. [8], simulations were performed to test the capabilities of RELXILL_NK in analyzing observations from *present* and *future* instruments. The constraints obtained there, simulating data with *present* instruments, are comparable with constraints obtained in the analysis here. This suggests that simulations are able to predict the capabilities of RELXILL_NK reasonably well. With X-ray missions like eXTP coming up [16], we are optimistic that the significantly better constraints obtained in simulations with *future* instruments will be realized in near future.

*Conclusions* — In this Letter, we have employed for the first time a new version of RELXILL designed to test the Kerr nature of astrophysical black holes to analyze *XMM-Newton*, *NuSTAR*, and *Swift* data of the supermassive black hole in 1H0707−495. We have chosen this source because the spectrum has a very strong iron K$\alpha$ line and the inner edge of the accretion disk extends up to very small radii. Our results are summarized in Tab. II and in Figs. 1 and 2, and are consistent with the assumption that the metric around the supermassive black hole in 1H0707−495 is described by the Kerr solution, as expected in general relativity. Work is currently underway to study other black holes with RELXILL_NK as well as to constrain other deformation parameters or to test black hole metrics from specific gravity theories.

*Acknowledgments* — Z.C. thanks the Cahill Center for Astronomy and Astrophysics at Caltech for hospitality during his visit where part of this work was done. The work of Z.C., S.N., and C.B. was supported by the National Natural Science Foundation of China (Grant No. U1531117) and Fudan University (Grant No. IDH1512060). C.B. and J.A.G. acknowledge the support from the Alexander von Humboldt Foundation.

[1] B. Carter, Phys. Rev. Lett. **26**, 331 (1971); D. C. Robinson, Phys. Rev. Lett. **34**, 905 (1975); P. T. Chrusciel, J. L. Costa and M. Heusler, Living Rev. Rel. **15**, 7 (2012).

[2] C. Bambi, *Black Holes: A Laboratory for Testing Strong Gravity* (Springer Singapore, 2017), doi:10.1007/978-981-10-4524-0

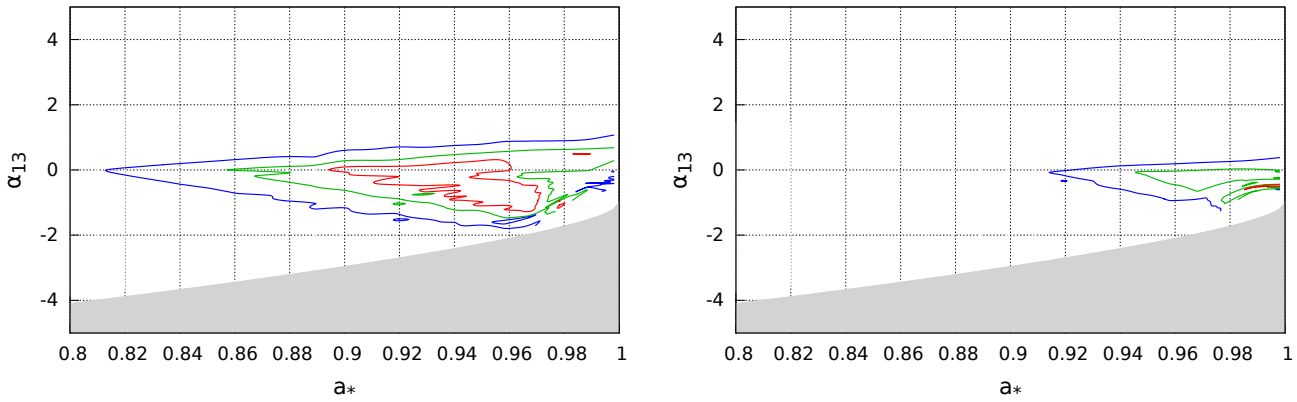


FIG. 1. Constraints on the spin parameter $a_*$ and the Johannsen deformation parameter $\alpha_{13}$ from the *XMM-Newton* data of 2011: Analysis 1 (left panel) and Analysis 2 (right panel). The red, green, and blue lines indicate, respectively, the 68%, 90%, and 99% confidence level curves for two relevant parameters. The grayed region is ignored in our study because it does not meet the condition in Eq. (3). See the text for more details.

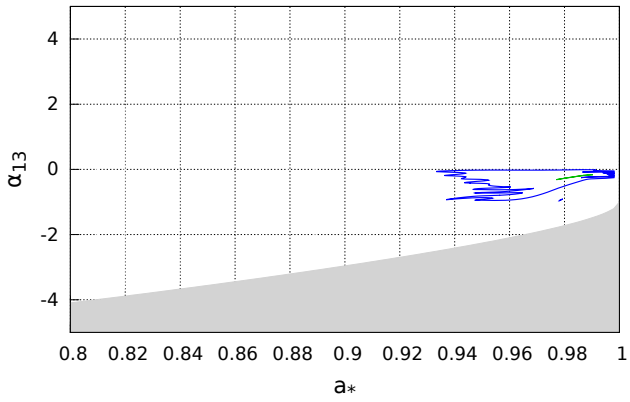


FIG. 2. As in Fig. 1 from Analysis 3 (*NuSTAR+Swift*). The 68% confidence level curve is too thin to be plotted. See the text for more details.


[3] C. M. Will, Living Rev. Rel. **17**, 4 (2014) [arXiv:1403.7377 [gr-qc]].

[4] C. Bambi, Rev. Mod. Phys. **89**, 025001 (2017) [arXiv:1509.03884 [gr-qc]].

[5] A. C. Fabian, K. Iwasawa, C. S. Reynolds and A. J. Young, Publ. Astron. Soc. Pac. **112**, 1145 (2000) [astro-ph/0004366]; L. W. Brenneman and C. S. Reynolds, Astrophys. J. **652**, 1028 (2006) [astro-ph/0608502]; C. S. Reynolds, Space Sci. Rev. **183**, 277 (2014) [arXiv:1302.3260 [astro-ph.HE]].

[6] J. Schee and Z. Stuchlik, Gen. Rel. Grav. **41**, 1795 (2009) [arXiv:0812.3017 [astro-ph]]; T. Johannsen and D. Psaltis, Astrophys. J. **773**, 57 (2013) [arXiv:1202.6069 [astro-ph.HE]]; C. Bambi, Phys. Rev. D **87**, 023007 (2013) [arXiv:1211.2513 [gr-qc]]; J. Jiang, C. Bambi and J. F. Steiner, Astrophys. J. **811**, 130 (2015) [arXiv:1504.01970 [gr-qc]]; C. Bambi, J. Jiang and J. F. Steiner, Class. Quant. Grav. **33**, 064001 (2016) [arXiv:1511.07587 [gr-qc]]; J. K. Hoormann, B. Beheshtipour and H. Krawczynski, Phys. Rev. D **93**, 044020 (2016) [arXiv:1601.02055 [astro-ph.HE]]; M. Zhou, A. Cardenas-Avendano, C. Bambi, B. Kleihaus and J. Kunz, Phys. Rev. D **94**, 024036 (2016) [arXiv:1603.07448 [gr-qc]]; Y. Ni, M. Zhou, A. Cardenas-Avendano, C. Bambi, C. A. R. Herdeiro and E. Radu, JCAP **1607**, 049 (2016) [arXiv:1606.04654 [gr-qc]]; C. Bambi, Z. Cao and L. Modesto, Phys. Rev. D **95**, 064006 (2017) [arXiv:1701.00226 [gr-qc]].

[7] T. Dauser, J. Garcia, J. Wilms, M. Bock, L. W. Brenneman, M. Falanga, K. Fukumura and C. S. Reynolds, Mon. Not. Roy. Astron. Soc. **430**, 1694 (2013) [arXiv:1301.4922 [astro-ph.HE]]; J. Garcia, T. Dauser, C. S. Reynolds, T. R. Kallman, J. E. McClintock, J. Wilms and W. Eikmann, Astrophys. J. **768**, 146 (2013) [arXiv:1303.2112 [astro-ph.HE]]; J. Garca *et al.*, Astrophys. J. **782**, 76 (2014) [arXiv:1312.3231 [astro-ph.HE]].

[8] C. Bambi, A. Cardenas-Avendano, T. Dauser, J. A. Garcia and S. Nampalliwar, Astrophys. J. **842**, 76 (2017) [arXiv:1607.00596 [gr-qc]].

[9] G. Matt, G. C. Perola and L. Piro, Astron. Astrophys. **247**, 25 (1991); A. Martocchia and G. Matt, Mon. Not. Roy. Astron. Soc. **282**, L53 (1996).

[10] T. Johannsen, Phys. Rev. D **88**, 044002 (2013) [arXiv:1501.02809 [gr-qc]].

[11] A. C. Fabian *et al.*, Nature **459**, 540 (2009) [arXiv:0905.4383 [astro-ph.HE]]; A. Zoghbi, A. Fabian, P. Uttley, G. Miniutti, L. Gallo, C. Reynolds, J. Miller and G. Ponti, Mon. Not. Roy. Astron. Soc. **401**, 2419 (2010) [arXiv:0910.0367 [astro-ph.HE]].

[12] A. C. Fabian *et al.*, Mon. Not. Roy. Astron. Soc. **419**, 116 (2012) [arXiv:1108.5988 [astro-ph.HE]].

[13] T. Dauser *et al.*, Mon. Not. Roy. Astron. Soc. **422**, 1914 (2012) [arXiv:1112.1796 [astro-ph.HE]].

[14] E. Kara *et al.*, Mon. Not. Roy. Astron. Soc. **449**, 234 (2015) [arXiv:1501.06849 [astro-ph.HE]].

[15] D. R. Wilkins, E. Kara, A. C. Fabian and L. C. Gallo, Mon. Not. Roy. Astron. Soc. **443**, 2746 (2014) [arXiv:1406.6658 [astro-ph.HE]].

[16] S. N. Zhang *et al.* [eXTP Collaboration], Proc. SPIE Int. Soc. Opt. Eng. **9905**, 99051Q (2016) [arXiv:1607.08823 [astro-ph.IM]].

## SUPPLEMENTAL MATERIAL

### *XMM-Newton* data

In the analysis of the 2011 *XMM-Newton* observation, we have only used the EPIC-pn data for simplicity. All data files were processed using XMM-Newton Science Analysis System SAS v16.0.0 and the current calibration files CCF updated to 14 March 2017. The spectra and light-curves were extracted using the tool *evselect* with default pattern. The source spectra were extracted from a circular region of radius of 35 arcsec and the background region was on the same chip. The effective area and redistribution matrix were produced by *arfgen* and *rmfgen*, respectively. EPIC-pn was in full window mode during the observation and no evidence of pile-up is found. All EPIC-pn spectra were then binned to a minimum of 20 photon counts per bin before analysis.

Fig. 3 shows the data and the data to model ratio of Analysis 1 (left panel) and Analysis 2 (right panel). While the minimum of the reduced $\chi^2$ is not very close to 1, the plots of the data to model ratio show that the fits are good. Note that the fits are driven by the small error bars form the soft energy band, but we know that the strong iron K$\alpha$ edge is there and therefore it is important to get the shape right as well. Fig. 4 shows the whole model (black line) and the two reflection components of Analysis 2; it can be compared with Fig. 5 in Ref. [12].

When we impose the Kerr metric ($\alpha_{13} = 0$), the best-fit values of some parameters are consistent with those found in Ref. [12], while others are not. However, there are several differences in the two analyses: we use different reflection models (RELXILL vs REFLIONX), some different input parameters (galactic dust absorption, redshift; we employ more recent measurements than [12]), and there are some differences in the data reduction and analysis. Our results are consistent with those found in Ref. [14], where, indeed, the differences listed above are not present.

### *NuSTAR*+*Swift* data

There are three separated *NuSTAR* observations of 1H0707−495 in 2014, with simultaneous snapshots of *Swift*/XRT. We did not include the second *Swift* observation in our analysis because it was during an anomaly period for the instrument. The *NuSTAR* data from both the FPMA and FPMB instruments were processed using nupipeline v0.4.5 with the standard filtering criteria and the NuSTAR CALDB version 20170120. For the spectra and light-curves extraction, we used the task *nuproduct* and we chose a circular source region of radius 40 arcsec and background region of radius 85 arcsec on the same chip. No pile-up effects were found in these *NuSTAR* observations. All spectra were binned to a minimum of 1 count before analysis. The *Swift*/XRT spectra were also extracted following the standard criteria with source region of radius 20 arcsec, using the *xselect* tool. The data were binned to a minimum of 1 count in order to do a simultaneous fitting with the *NuSTAR* observations. Since the signal is low, we used the Cash-statistics in the analysis of the *NuSTAR*+*Swift* data.

Fig. 5 shows the data to model ratio of Analysis 3 *NuSTAR*+*Swift* (left panel) and the energy$^2$ $\cdot$ model and the data to model ratio of the *NuSTAR* data only (right panel). The right panel in Fig. 5 can be compared with Fig. 3 in Ref. [14].

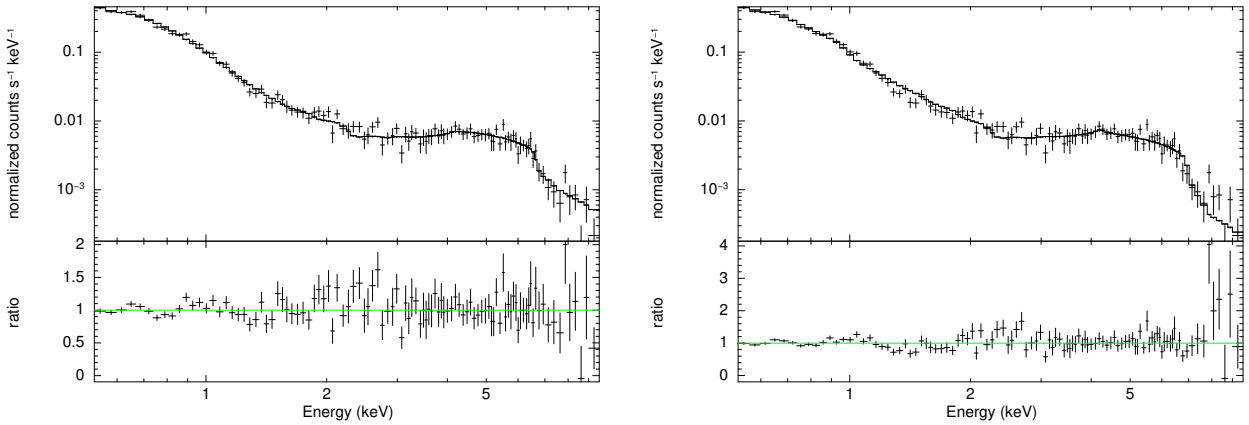


FIG. 3. Data and data-to-model ratio of the *XMM-Newton* observation of 2011: Analysis 1 (left panel) and Analysis 2 (right panel).

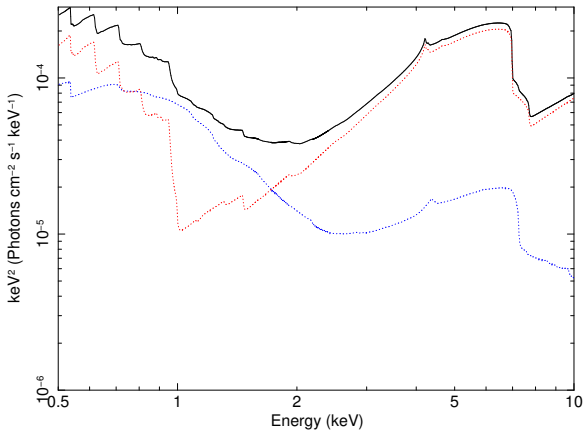


FIG. 4. energy$^2$ $\cdot$ model for Analysis 2. The red and blue lines are the reflection components with, respectively, lower and higher value of $\xi$. The black line is the whole model.

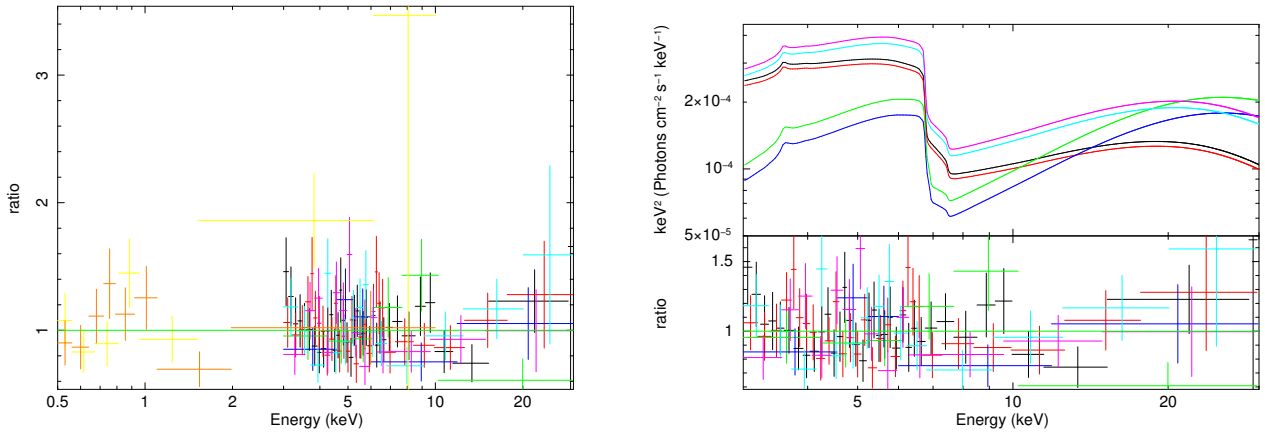


FIG. 5. Left panel: Data-to-model ratio of the *NuSTAR*+*Swift* observations of 2014 corresponding to Analysis 3. Right panel: energy$^2$ · model and the data to model ratio of the *NuSTAR* observations only; for every observation, we have both the FPMA and FPMB data sets. The data have been rebinned for plotting purposes only.